Anticipating Collisions, Navigating in Complex Environments, Elbowing, Pushing, and Smartphone-Walking: A Versatile Agent-Based Model for Pedestrian Dynamics

Iñaki Echeverría-Huarte, Alexandre Nicolas

Anticipating Collisions, Navigating in Complex Environments, Elbowing, Pushing, and Smartphone-Walking: A Versatile Agent-Based Model for Pedestrian Dynamics

Iñaki ECHEVERRÍA-HUARTE*
Departamento de Física y Matemática Aplicada, Facultad de Ciencias, Universidad de Navarra, 31080 Pamplona, Spain.

Alexandre NICOLAS†
Institut Lumière Matière, CNRS & Université Claude Bernard Lyon 1, 69622 Villeurbanne, France.

(Dated: November 4, 2022)

Compared to other self-propelled particles, pedestrians are able to anticipate, which gives them an edge in avoiding collisions and navigating in cluttered spaces. These capabilities are impaired by digital distraction through smartphones, a growing safety concern. To capture these features, we put forward a continuous agent-based model hinging on a transparent delineation of a decision-making process and a mechanical layer that handles contacts and collisions. In the decisional layer, each agent autonomously selects their desired velocity as the optimum of a perceived cost, notably balancing the will to move forward (described by a floor field) with the bio-mechanical cost of walking and the risk of collision, assessed by an anticipated time-to-collision. Altogether, the model includes less than a dozen parameters, most of which are fit using independent experimental data.

Numerical simulations demonstrate the versatility of the approach, which succeeds in reproducing empirical observations in extremely diverse scenarios, often quantitatively, with a single set of parameters. These scenarios range from collision avoidance involving one, two, or more agents to collective flow properties in unidirectional and bidirectional settings and to the dynamics of evacuation through a bottleneck, where contact forces are directly accessible. Remarkably, a straightforward transcription of digital distraction into the model, by reducing the frequency of decisional updates, suffices to replicate the enhanced chaoticity of the flow, with more frequent sudden turns, observed experimentally when 'smartphone-walking' pedestrians are brought in.

Finally, the conceptual transparency of the model makes it easy to pinpoint the origin of some deficiencies, notably its short-sighted account of anticipation (when agents have to cross a group of people) and the disk-like pedestrian shape (when very dense crowds are considered). Our work thus clarifies the singular position of pedestrian crowds in the midst of active-matter systems.

I. INTRODUCTION

Pedestrians routinely display remarkable navigation and coordination abilities, which enable them to adapt to new environments, make their way through dense crowds [1, 2] and navigate in very constrained surroundings. But, like Marcus Aurelius's infallible man [3], the infallible pedestrian simply does not exist: Suboptimal routing choices [4], collisions, or even in the most tragic cases stampedes [5] are indeed also prominent features of crowd dynamics. Uncoordinated behavior gets even more visible in our overly connected societies, where the pedestrians' attention to their surroundings are often diverted by their smartphones [6, 7]. Crowds may thus display both high abilities for self-organization and individualistic choices conducive to undesirable collective effects. Models capable of capturing this somewhat contradictory alliance would be highly beneficial for practical purposes, of course, when it comes to designing new pedestrian facilities [8], but also more fundamentally, to disentangle the specifics of pedestrian dynamics from the roots they share with other physical assemblies, notably active matter. At present, these antagonistic features are, to say the least, only dimly reflected in the vast array of (continuous) microscopic models for crowd dynamics. Schematically, one branch of models prohibits the selection of all velocities potentially leading to a collision, whereas a second branch handles collision avoidance as a repulsive force.

The first branch (typically comprised of velocity-based models) was largely inspired by the field of robotics [9–11] in an endeavor to guarantee collision-free motion of multiple agents [12]. If it is implemented in a fully decentralized way, this approach tends to be overly conservative ('prudent') and too often the dynamics get frozen (deadlocks) or look unnatural in the presence of conflicting maneuvers [13]. To circumvent this issue, global coordination of individual moves may be enforced via a more or less centralized process [12, 14]. This leads to reasonable output for a variety of situations, but may arguably not be scalable to large crowds (involving thousands of pedestrians). Furthermore, the predicted trajectories tend to look too 'robotic' (with sharp turns, etc.) [13]. The prediction of the other agents' trajectories, mediated by perception, can also be enforced in a context-dependent way [15] and bring the agents' behavior closer to human response, but at the risk of requiring a different treatment for every situation and making them less amenable to theoretical understanding.

At the other extreme, in the wake of the celebrated

* iecheverria.13@alumni.unav.es
† alexandre.nicolas@polytechnique.edu

Social Force Model [16], force-based models hypothesize that the local rules of navigation can be represented by *ad hoc* pseudo-forces encoding 'intuitive' social interactions (such as keeping some distance from one another via a repulsive or walking in a group via an attractive interaction [17]) and inserted into an e.g. Newton-like equation of motion, along with mechanical forces. This particle-based approach has succeeded in replicating various collective and/or self-organized phenomena in crowds [18], but is also known to lead to spurious oscillations [19] and to deadlocks or conflicts caused by an unrealistic lack of anticipation by the agents. These issues are partly remedied by supplementing the models with specific forces enforcing a following or an anticipatory behavior [13, 20]. In a study of note, Karamouzas et al. showed that the empirical collision avoidance behaviour depends on the anticipated time to collision (TTC), rather than on the absolute distance r between people and is thus better described by an interaction depending on the TTC than on r [21]. Other anticipatory behaviors and follow-the-leader rules have also recently been put forward [13, 20]. But this remedial process is essentially *ad hoc* and adds patches to an existing model without fundamentally questioning its overall structure.

In this paper, we propound a modeling framework that mirrors the main processes involved in pedestrian motion, whereby each agent updates their desired velocity via a decision-making process that optimizes a pseudo-energy (or perceived cost) [22], notably comprising a TTC term to render collision avoidance [21], whereas the contacts and pushes that may ensue are handled by a mechanical layer (Sec. II). Thanks to the transparent coincidence between the building blocks and the processes they describe, most model parameters can be calibrated independently. Inherently decentralized, the algorithm reproduces realistic collision avoidance in crowds and coordinated motion in crowded scenarios as well as other collective effects, in quantitative agreement with experimental data, using a single set of parameters for the different regimes under study (Sec. III). The model can further straightforwardly be extended to account for 'smartphone-walking', which has become a serious practical issue. The relative simplicity of the proposed framework makes it suitable for physical insight into the similarities and discrepancies with other types of active matter.

II. MODELING FRAMEWORK

A. Decision-making layer and mechanical layer

A pedestrian is both an autonomous agent that controls his or her motion and a physical body that evolves in a mechanical environment. In the parlance of control theory, a pedestrian is thus *both* the 'controller' and the 'system' responding to the control signal. These two roles are amalgamated in most microscopic models for pedestrian motion [19] and, more generally, active matter, in which a single equation governs the evolution of the actual velocity of the agent. Here, to mimic the sequential process at play in human locomotion, we choose to clearly disentangle the decision-making process, whereby the agent selects a desired velocity, from the mechanical block governing the response of the pedestrian's body in interaction with the environment.

In the rest of this section, we successively introduce the decisional layer [10, 22, 23] and the mechanical one.

B. Decision-making layer

The move (consciously or unconsciously) chosen by a pedestrian at each time step can be regarded as an optimum over a set of options from the viewpoint of this agent. Optimality, in this sense, is typically defined in rational choice theory as the maximization of a utility function or equivalently the minimization of a perceived cost function $\mathcal{E}$. As a matter of fact, the choice need not be wholly rational: the cost function may be purely subjective and affected by the bounded rationality of the agents or the limited information available to them. Such an approach has previously been applied to select an optimal step [24], but here we apply it for the choice of a desired velocity $\boldsymbol{u}^\star$ for the next time step, viz.

$$\boldsymbol{u}^\star = \underset{\boldsymbol{u}\in\mathbb{R}^2}{\operatorname{argmin}}\ \mathcal{E}(\boldsymbol{u}). \tag{1}$$

From a broader perspective, this criterion can be interpreted as an optimal control problem over a very small time horizon δt (where δt is the interval between decisions, due to the reaction time), in which one would like to extremize

$$\mathcal{E}[\boldsymbol{u}] \;=\; \underbrace{\int_t^{t+\delta t} e\left(t', \boldsymbol{r}(t'), \boldsymbol{u}(t')\right) dt'}_{\text{running cost}} + \underbrace{\mathcal{E}^{\mathrm{T}}\left(\boldsymbol{r}(t+\delta t)\right)}_{\text{terminal cost}}$$

$$\mathcal{E}(\boldsymbol{u}) \overset{\delta t\to 0}{\approx} \delta t\, e\left(t, \boldsymbol{r}(t), \boldsymbol{u}\right) + \mathcal{E}^{\mathrm{T}}\left(\boldsymbol{r}(t) + \delta t\, \boldsymbol{u}\right) \tag{2}$$

The foregoing formula is reminiscent of the least action principle for a physical system, whereby the trajectory selected by nature minimizes a quantity called the action (also see [25] for an application to dilute pedestrian flows). But, crucially, the cost is here minimized by each agent separately, knowing some information about the others, and not globally by the whole assembly, as in previous endeavors [14]. This reflects the autonomous nature of the agents and drives a wedge between social assemblies and physical systems.

Let us now detail the various terms contributing to the perceived cost $\mathcal{E}(\boldsymbol{u})$.

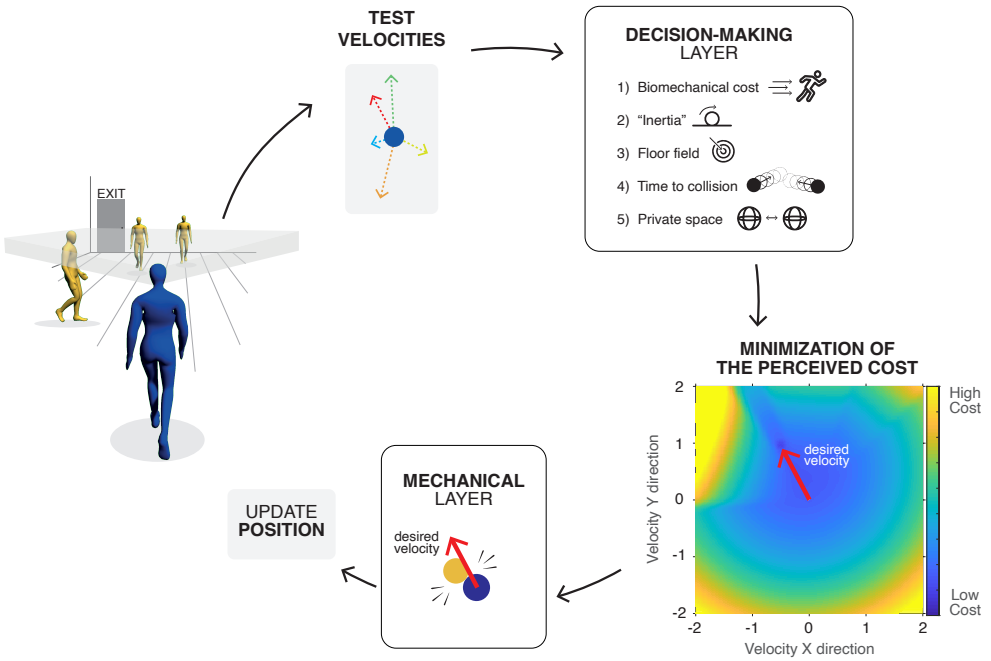

FIG. 1. Schematic representation of the algorithm. Every time step δt, the agent collects information about the environment and the other agents in his or her field of view (left), considers various test velocities and selects the optimal one from the perspective of his/her perceived cost. The self-propulsion force corresponding to this desired velocity is implemented in the mechanical layer, which handles possible contacts or collisions and returns the agent's updated position.

1. *Static floor field*

In Eq. 2, the driving term, which accounts for the desire to move towards a target destination, is the terminal cost $\mathcal{E}^{\mathrm{T}}$, which is a function of the expected position $\boldsymbol{r'}$ at time $t+\delta t$: The closer one gets to the target, the better. This term is manifestly related to the pedestrian's motivation, and thus of psychological origin. We shall adopt the simplest possible approach and assume that $\mathcal{E}^{\mathrm{T}}(\boldsymbol{r'})$ is a static (i.e., time-independent) floor field that grows linearly with the shortest-path distance $\mathcal{D}(\boldsymbol{r'})$ between $\boldsymbol{r'}$ and the agent's target. These distances are defined by the Eikonal equation $|\nabla_{\boldsymbol{r}}\mathcal{D}| = n(\boldsymbol{r})$ generally used for ray tracing. Here, the 'refractive index' $n(\boldsymbol{r})$ measures how uncomfortable the environment at $\boldsymbol{r}$ is. In particular, while $n = 1$ in free space, proximity to a wall is penalized by the function $n(\boldsymbol{r}) = \tanh^{-1}(d_w(\boldsymbol{r})/d_c)$, where $d_w(\boldsymbol{r})$ denotes the distance to the closest wall and the repulsive length d_c (typically 20 cm in the following) is a parameter of the model. Overall, the floor field thus reads

$$\mathcal{E}^{\mathrm{T}}(\boldsymbol{r'}) = \frac{K^T}{n}\,\mathcal{D}(\boldsymbol{r'}), \tag{3}$$

where $K^T > 0$ is a coefficient which, for reasons that will soon transpire (Sec. II B 2), we have chosen to divide by the 'refractive index' $n = n(\boldsymbol{r})$. Note that $n(\boldsymbol{r})$ in Eq. 3 may vary with the agent's current location $\boldsymbol{r}$, but on no account not with the test velocity $\boldsymbol{u}$ or the test position $\boldsymbol{r'} = \boldsymbol{r} + \delta t\,\boldsymbol{u}$. Importantly, using a floor field in this continuous model circumvents the practical issues typically associated with the definition of standard road maps (i.e., 'central' paths) that agents have to follow indiscriminately or the nontrivial prescription of a field of desired velocities in a complex geometry, which is here handled straightforwardly (see Sec. III C).

Technically speaking, the shortest-path distances $\mathcal{D}$ are computed on a hexagonal lattice (the dual of a honeycomb lattice) before runtime and stored in memory. This is done by means of Dijkstra's algorithm, considering the nearest two neighbors of each node and evaluating the cost $n(\boldsymbol{r})$ of traveling along an edge at the next (rather than current) node. The use of a highly symmetric hexagonal lattice strongly curbs the spurious anisotropy that is known to be generated by the Dijkstra algorithm (e.g., on square lattices); in practice, the variations of the free walking speed with the direction of motion are reduced to less than 10%.

2. *Bio-mechanical cost associated with walking speed and 'inertia'*

The target cannot be reached instantly: The locomotive abilities of pedestrians constrain the choice of a desired velocity $\boldsymbol{u}^\star$. The faster one moves, the more energy is consumed by the body. The bio-mechanical dependence of this energy e^{speed} on speed $u = ||\boldsymbol{u}||$, which

is internalized in the decision-making process, has been quantitatively assessed via measurements of oxygen consumption (e.g., of participants walking on a treadmill) [26]; the excess energy expenditure compared to rest comprises a constant (penalty for walking) plus a term which grows as the square of u multiplied by a height-dependent prefactor.

We choose to discard the base energy consumption at rest and to connect the curve smoothly to 0 when $u \to 0$, i.e., have $e^{\text{speed}}(u)$ vanish when an agent halts, arriving at the following equation (refer to Appendix A for details), which nicely fits the experimental data of [26], as shown in Fig. 2,

$$e^{\text{speed}}(u) = \begin{cases} 7.6\,u - 35.4\,u^2 & \text{for } u < 0.1\,\text{m}\cdot\text{s}^{-1} \\ 0.4 + 0.6\,u^2 & \text{for } u \geqslant 0.1\,\text{m}\cdot\text{s}^{-1}. \end{cases} \quad (4)$$

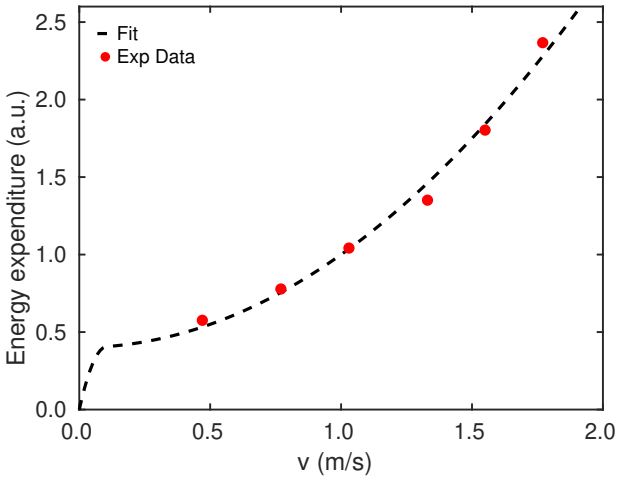

FIG. 2. Bio-mechanical cost e^{speed} associated with the walking speed v in the model, given by Eq. 4, and comparison to the aggregated data of [26] (adult group).

Besides, abrupt changes in velocity should also be barred because they are uncomfortable and bio-mechanically costly, which suggests an 'inertial' contribution

$$e^{\text{inertia}}(\boldsymbol{u}) = \mu\Big(\boldsymbol{u} - \boldsymbol{v}(t)\Big)^2, \quad (5)$$

where $\boldsymbol{v}(t)$ is the actual velocity at time t and $\boldsymbol{u}$, the test velocity for the next time step, $t + \delta t$, and $\mu > 0$.

Without any further contributions (from the environment), the extremum of $\mathcal{E}(\boldsymbol{u}) = \delta t\Big[e^{\text{speed}}(\boldsymbol{u}) + e^{\text{inertia}}(\boldsymbol{u})\Big] + \mathcal{E}^T(\boldsymbol{r} + \delta t\,\boldsymbol{u})$ is reached when

$$0 = \frac{1}{\delta t}\nabla_{\boldsymbol{u}}\mathcal{E} = 2\,\mu\Big(\boldsymbol{u} - \boldsymbol{v}(t)\Big) + \frac{de^{\text{speed}}}{du}\frac{\boldsymbol{u}}{u} - K^T\,\boldsymbol{t}, \quad (6)$$

where $\boldsymbol{t} = -\nabla_{\boldsymbol{r}}\mathcal{D}/n(\boldsymbol{r})$ is a unit vector pointing towards the target, in free space. Hence, the free walking speed *in steady state* is $u^\infty = K^T/1.2$, for $u \geqslant 0.1\,\text{m}\cdot\text{s}^{-1}$ (details can be found in Appendix B). Provided that u^∞ is empirically known (typically between 1.2 and 1.8 m/s depending on the situation), the parameter K^T can be set straightforwardly.

Strikingly, since $\boldsymbol{u}$ is the desired velocity at $t+\delta t$, Eq. 6 is formally identical to the numerical resolution of Newton's second law with a forward Euler scheme [14]. At this stage, we should underscore the two key conceptual shifts that have been made so far with respect to most existing models. First, Newton's equation is not obtained by dint of some fundamental physical law, but because of the simple form chosen for e^{inertia} in the decisional layer. Second, the free walking speed u^∞ explicitly results from the balance between a bio-mechanical cost e^{speed}, that may vary with the pedestrian but not with the context, and a will to move described by the terminal cost (or floor field) $\mathcal{E}^T$; all psychological and motivational effects (heightened in the event of an emergency, for instance) are deferred to $\mathcal{E}^T$. This makes sense, because $\mathcal{E}^T$ also governs the route choice.

3. *Private space*

Another intuitive contribution comes from the desire not to stand excessively close to other pedestrians or obstacles, i.e., to preserve one's private space, the dimensions of which vary between cultures [27]. Here, it is modeled as a distance-dependent repulsive term entering the terminal cost in Eq. 2,

$$\mathcal{E}^{\text{private}}(\boldsymbol{r}') = \sum_{j \in f.o.v.(i)} \frac{\eta}{\sigma_i + \sigma_j} V^{\text{rep}}\Big(\frac{||\boldsymbol{r}' - \boldsymbol{r}_j(t+\delta t)||}{\sigma_i + \sigma_j}\Big), \quad (7)$$

where $\boldsymbol{r}_j(t+\delta t) = \boldsymbol{r}_j(t) + \delta t\,\boldsymbol{v}_j(t)$ is the expected position of agent j at the next time step, σ_j is the radius of agent j, and V^{rep} is a short-ranged function. We cut if off at $1 + \epsilon^\star$, where $\epsilon^\star \geqslant 0$, and set

$$V^{\text{rep}}(\tilde{r}) = \begin{cases} \frac{1}{\tilde{r}} - \frac{1}{1+\epsilon^\star} & \text{if } \tilde{r} < 1 + \epsilon^\star \\ 0 & \text{otherwise.} \end{cases} \quad (8)$$

To account for perception, in Eq. 7, the sum does not run over all neighboring agents j, but is limited to those in the *field of view* (f.o.v.) of the agent (i), i.e., within a cone which extends from $-\theta$ to $+\theta$ around the direction of the agent's last desired velocity $\boldsymbol{u}(t)$.

4. *Time-to-collision (TTC) energy*

All contributions so far are based on positions and distances, possibly anticipated at the next time step $t + \delta t$. This was argued to give an inadequate reflection of the cognitive heuristics employed by humans for collision

avoidance [22]. Indeed, as later shown by Karamouzas et al. [21], the positional variables are not well suited to describe the spacing distances between pedestrians (notably resulting from their mutual avoidances) and had better be substituted by an anticipated time to collision (TTC), which is the earliest time $\tau_{ij} \in (0, \infty)$ at which agents i and j are expected to collide. τ_{ij} can readily be calculated if agents j are handled as disks of radii σ_j and agent i assumes that all neighbors j maintain their current velocities. Then, the TTC reads [14]

$$\tau_{ij}(\boldsymbol{u}_i) = \frac{-\boldsymbol{x}_{ij} \cdot \boldsymbol{v}_{ij} - \sqrt{\Delta}}{v_{ij}} \tag{9}$$

if $\Delta = (\boldsymbol{x}_{ij} \cdot \boldsymbol{v}_{ij})^2 - v_{ij}^2[x_{ij}^2 - (\sigma_i + \sigma_j)^2] \geqslant 0$, or ∞ otherwise. Here, $\boldsymbol{x}_{ij}$ and $\boldsymbol{v}_{ij}$ are the relative positions and desired velocities of i with respect to j.

In the light of empirical data on interpedestrian spacings, Karamouzas et al. [21] established an interaction potential

$$V^{TTC}(\tau) = K^{TTC} \frac{\exp(-\tau/\tau_c)}{\tau^p}, \tag{10}$$

where $p = 2$; τ_c was set to 3.0 s.

In our case, unlike Karamouzas et al. [14, 21], only the most imminent collision risk, i.e., the shortest TTC, will be considered by each agent, viz.

$$e^{TTC} = \max_{j \in f.o.v.(i)} \underbrace{V^{TTC}\Big[\tau_{ij}(\boldsymbol{u}_i)\Big]}_{\equiv e_j^{TTC}}. \tag{11}$$

This focus on only the most imminent collision vaguely echoes Primo Levi's impression (in an admittedly wholly unrelated context [28]) that one experiences fears and pains one at a time, the most acute coming first, as though the smaller ones remained hidden behind it while it persists. Moreover, as previously, the agents fields of view restrict the set of neighbors that they actually see; the TTC of agents out of their f.o.v. is regarded as infinite.

So far, the TTC energy penalizes desired velocities that lead to physical contact. However, pedestrians are also eager to avoid encroachments on their private spaces. Suppose that the private space is a disk of radius $(1+\epsilon)\sigma_i$, where $\epsilon \geqslant 0$ and σ_i is the body radius of the agent (i, here). Equation 9 can then be applied to retrieve the TTC of private spaces, $\tau_{ij}(\epsilon)$, provided that the sum of body radii $\sigma_i + \sigma_j$ is multiplied ('inflated') by $1 + \epsilon$.

Since the transition into the private space is actually smooth, the TTC energy will read

$$e_j^{TTC} = \frac{\int_0^\infty V^{\text{rep}}(1+\epsilon)\, V^{TTC}[\tau_{ij}(\epsilon)]\, d\epsilon}{\int_0^\infty V^{\text{rep}}(1+\epsilon)\, d\epsilon}. \tag{12}$$

For simplicity, as well as computational efficiency, in practice we will approximate the foregoing formula by

$$e_j^{TTC} = \frac{1}{\epsilon_i^\star} \int_0^{\epsilon_i^\star} V^{TTC}[\tau_{ij}(\epsilon)]\, d\epsilon \tag{13}$$

Here, $\epsilon_i^\star = \min\Big(\epsilon^\star, \epsilon_i\Big)$ may be lower than the maximal extent of the private space, $\epsilon^\star$, if this value leads to an overlap of the private sphere at the present time; in that case, $\epsilon_i^\star$ is capped to ϵ_i, the largest inflation factor guaranteeing that agent i's private space does not currently overlap any other agent's. A similar averaging procedure was put forward in [29] to smooth the TTC energy (with respect to positions), but it was then interpreted as the result of an uncertainty on the evaluation of body sizes.

If no collision with agent j is ever expected, even with maximally inflated radii, i.e., $\tau_{ij}(\epsilon_i^\star) = \infty$, then $e_j^{TTC} = 0$. Otherwise, the minimal inflation leading to collision, $\epsilon_{ij}^c \geq 0$, can easily be derived from Eq. 9. Equation 13 is further approximated by

$$e_j^{TTC} \approx \frac{\epsilon_i^\star - \epsilon_{ij}^c}{\epsilon_i^\star}\, V^{TTC}\Big[\tau_{ij}\Big(\frac{\epsilon_i^\star + \epsilon_i^c}{2}\Big)\Big]. \tag{14}$$

TTC-based anticipation is also operational with respect to walls, but their linear shape modifies the technical calculation of the TTC. More specifically, the TTC τ_{iw} is defined as the shortest time after which the disk representing the agent would collide with a linear segment of a wall, if it moves at the test velocity $\boldsymbol{u}$; no private space is considered in this case (recall however from Sec. II B 1 that the proximity to walls in penalized in the floor field).

This concludes the summary of the pseudo-energies entering the perceived cost function

$$\mathcal{E}(\boldsymbol{u}) = \mathcal{E}^T\Big[\boldsymbol{r}(t) + \delta t\, \boldsymbol{u}\Big] + \mathcal{E}^{\text{private}}\Big[\boldsymbol{r}(t) + \delta t\, \boldsymbol{u}\Big] + \delta t\, \Big[e^{\text{speed}}(u) + e^{\text{inertia}}(\boldsymbol{u}) + e^{\text{TTC}}(\boldsymbol{u})\Big],$$

whose minimization, performed using a Nelder-Mead algorithm [30], yields the desired velocity $\boldsymbol{u}^\star$, for each agent.

C. Mechanical contacts

Collisions between pedestrians are rare, but may occur in very dense crowds. In that case, should the desired velocity $\boldsymbol{u}_i^\star$ lead to a collision within the decisional update time δt, these collisions are handled within our model by a mechanical 'layer' (see Fig. 1), which solves Newton's equations [31]

$$\ddot{\boldsymbol{r}}_i = \frac{\boldsymbol{u}_i^\star - \dot{\boldsymbol{r}}_i}{\tau^{\text{mech}}} + \frac{1}{m}\sum_j \boldsymbol{F}_{j\to i}^{\text{Hertz}} + \frac{1}{m}\sum_{w \in \text{walls}} \boldsymbol{F}_{w\to i}^{\text{Hertz}}, \tag{15}$$

Symbol	Definition	Value
Decision-making layer		
δt	Decision-making time	0.1 s
u^∞	Preferential speed, or free-walking speed	1.0-2.0 m/s
μ	Inertial coefficient	0.01
η	Repulsive coefficient associated with private space	0.8
ϵ	Spatial extent of the private space (relative to body width)	0.2
d_c	Characteristic repulsion length of walls	20 cm
θ	Visual cone (half-angle)	70°
Mechanical layer		
τ^{mech}	Relaxation time	0.2 s
κ/m	Renormalized body stiffness	10^6

TABLE I. Definitions and values of the model parameters. Note that δt is chosen somewhat shorter than the reaction time to complex stimuli, because the human decision-making process is more sophisticated than that modeled here.

wherein agents self-propel in the direction of their desired velocity $\boldsymbol{u}_i^\star$, which they reach in a characteristic time $\tau^{\text{mech}} \approx 0.2\,\text{s}$ in free space. Besides, they are assumed to interact with each other via frictionless Hertzian contact forces $\boldsymbol{F}_{j\to i}^{\text{Hertz}} = \kappa\, P\Big(\frac{\sigma_i+\sigma_j}{r_{ij}} - 1\Big)\,(\boldsymbol{r}_i - \boldsymbol{r}_j)$, where $P(x) = \max(0, x)$, as though they were homogeneous elastic cylinders of radii σ_i and σ_j with parallel axes. Similarly, contacts with a wall w result in a force $\boldsymbol{F}_{w\to i}^{\text{Hertz}} = \kappa\, P\Big(\frac{\sigma_i}{r_{iw}} - 1\Big)\,(\boldsymbol{r}_i - \boldsymbol{r}_w)$, where $\boldsymbol{r}_w$ is the wall point closest to i and r_{iw} is the distance to the wall. Numerically, Eq. 15 is solved with a velocity Verlet algorithm, using a typical time step $dt = 2 \cdot 10^{-4}$.

Of course, the present mechanical description ought to be refined in the future, turning to more realistic shapes and interactions for the agents. These improvements can easily be integrated within the sturdy theoretical ground outlined here, which already convincingly describes many features of pedestrian dynamics, as exposed in the next section.

III. RESULTS

This section evinces that, despite its simplicity, the model introduced previously succeeds in quantitatively reproducing empirically observed features. Most importantly, although these situations cover a wide range of contexts and densities, no adjustment of the main parameter set (apart from very marginal ones required by the context) is required. We will initially validate the algorithm at the individual level and then move to collective properties.

In the following simulations, we used the main model parameters detailed in Table. I. Regarding the pedestrian shapes, whenever *crowds* are simulated, their body radii will be chosen in a normal distribution of mean 22.5 cm and standard deviation 2 cm. The preferential speeds will typically be normally distributed around $u^\infty = 1.4 \pm 0.2\ \text{m}\cdot\text{s}^{-1}$, but bounded below by $1.0\ \text{m}\cdot\text{s}^{-1}$.

A. Collision avoidance by a single pedestrian

Since a distinctive feature of pedestrian dynamics is anticipated collision avoidance, we begin by probing binary avoidance maneuvers involving two pedestrians (body radius: $r_p = 25\,\text{cm}$, preferential speed: $1.4\,\text{m}\cdot\text{s}^{-1}$) in a 10 m length and 3 m width corridor, in the two simple setups studied experimentally by Moussaid et al. [32]. In the first setup (top of Fig. 3), one pedestrian stands still in the center of the corridor, at $(X, Y)(0, 0)$. Meanwhile, the other one is asked to cross the corridor from an initial position at $X = -5\,\text{m}$, $Y \in [-r_p, r_p]$ to a distant target zone centered at $(X = 5\,\text{m}, Y = 0, \text{m})$, avoiding this 'obstacle' (first part of Supplementary Video I). Mostly by adjusting the inertial coefficient μ, we manage to obtain a close-to-perfect agreement between the model output and the average experimental behavior, apart from the avoidance-side preference (which is overlooked in the model and washed out of the experiments by plotting the absolute transverse displacements $|Y|$ instead of Y). The quality of the fit may even surpass that obtained with a social force model specifically calibrated for these experiments in the seminal original paper [32].

In the second setup (bottom of Fig. 3), the pedestrians are initially at opposite ends of the corridor ($X = \pm 5\,\text{m}$, $Y \in [-r_p, r_p]$) and walk in opposite directions. They start deviating from the central line already 3 meters ahead of the point of encounter (so typically 6 meters away from their counterpart). The maximal transverse displacement, at the point of encounter, appears to be smaller than in the first setup with the static obstacle ($Y \approx 50\,\text{cm}$), but one must bear in mind that, in this second setting, the workload associated with the avoidance maneuver is shared by two pedestrians, so that their separation distance on the crossing line is comparable to that observed when one of them stands still (second part of Supplementary Video I); the deviation is however undertaken earlier in the second setting, in line with the expectations based on the TTC. It is noteworthy that the (statically averaged) experimental trajectories are almost perfectly reproduced, without further adjustment compared to the first case. Of course, this comparison is oblivious to the avoidance-side bias observed experimentally, for which we did not introduce any counterpart in the model.

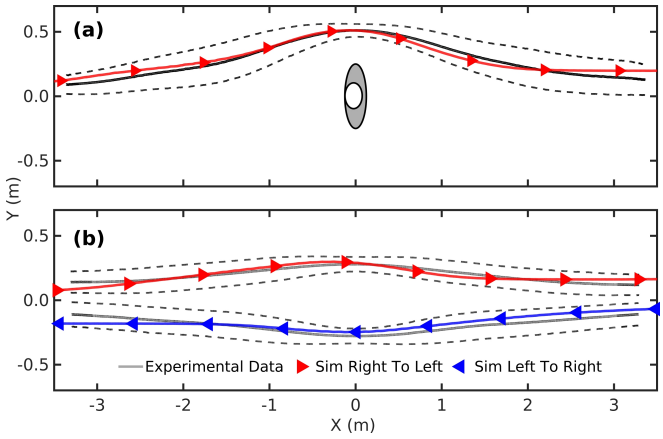

FIG. 3. Avoidance maneuvers between in a corridor: (top) Avoidance of a still-standing pedestrian 'obstacle' at the center; (bottom) trajectories of two counter-walking pedestrians. The computer simulations (coloured lines) are compared to the experiments (grey lines); the dashed lines materialize an envelope of width the standard deviation on each side of the moving average (solid line). The experimental trajectories were shifted along Y to start at $Y = 0$.

B. Many-body collision avoidances: Antipodal experiment on a circle

Having validated the model for two-body interactions, we move on to the interactions among a larger number of people. Circle antipodal experiments are an archetypal way to probe many-body collision avoidances. In this configuration, pedestrians are initially positioned on a circle (of 5 or 10 m of radius for example [33]) with uniform spacing between them and instructed to quickly reach the antipodal positions as soon as a signal is heard. Were they to walk straight to their targets at equal speeds, they would meet at the centre of the circle. Instead, experiments have shown that they deviate from the plain straight path soon after setting in motion. By adopting various collision avoidance and detour strategies, they manage to reach their target without substantial near collisions, even when there are up to 64 participants walking simultaneously [33]. We replicated the experimental setup numerically for a set of 8 agents with normal preferential speeds. Without mutual interactions, these agents would walk straight ahead at very similar speeds, despite their different directions, thanks to our use of a hexagonal lattice for the floor field (as we explained in Sec. II B 1). Instead, we observe that they deviate from the straight path and easily manage to reach the antipodal position (see the video in the Supplemental Material). The simulated trajectories are smooth and, as in the experiments, they do not excessively concentrate at the conflict-rife center of the circle; this is at odds with the output of the social force model, either in its traditional version or in a specifically designed variant, which were both deemed to significantly differ from the experimental results in [33]. Nevertheless, on account of the high variability between individuals and realizations, we have not sought a more quantitative comparison of trajectories here and have settled with the foregoing appreciation of the visual realism of the model output.

Another opportunity to study many-body collision avoidance is afforded by interweaving pedestrian flows, in which non-parallel streams of pedestrians are forced to cross; however, the individual pedestrian behaviors observed experimentally [34] are even more varied than in the antipodal experiments. Nevertheless, Luan et al. disclosed four major individual avoidance strategies [34]; let us briefly inquire into their compatibility with our model. To evade a collision, pedestrians may accelerate (strategy 1) or decelerate (strategy 2), come to a full halt (strategy 3), or make a detour to avoid a collision (strategy 4). Suppose that a simulated agent anticipates a collision in the direction $\boldsymbol{t}$ if he or she walks at a speed $u = u^\infty$; for this agent, the bio-mechanical cost e^{speed} or terminal cost $\mathcal{E}^T$ of accelerating ($u > u^\infty$) or decelerating ($u < u^\infty$) with respect to the preferential speed u^∞ is most often compensated by the ensuing reduction in TTC energy $e^{TTC}(u\boldsymbol{t})$, so the first two strategies are clearly within the reach of the model. So is the third one, namely coming to a full halt, which is but a special case of strategy 2; indeed, standing still has a lower bio-mechanical cost e^{speed} than moving (Fig. 2). Making a detour (strategy 4) is also widely observed within the frame of our model, as already reported for the binary collision avoidance (Sec. III A) and the antipodal scenario, especially when modifying one's speed is not enough to avoid a collision. (On the other hand, accelerating during this detour, which was often observed experimentally [34], will only be undertaken by the simulated agents if the detour alone does not ward off the risk of collision; otherwise, the less favorable walking direction during the detour results in lower gains in the terminal cost for moving forward, hence a lower propensity to walk fast.)

C. Navigation in a complex geometry

Navigation in a complex environment adds another layer of complexity to the foregoing multi-agent scenarios, in that each agent must also interact with the built environment. To characterize pedestrian flows in these (practically relevant) situations, we designed a geometry very loosely inspired from the ground floor of Montparnasse train station in Paris, France, in which about 100 pedestrians (with a lower threshold on preferential speeds set to $u^\infty = 1.2\,\text{m/s}$), classified in 7 groups with distinct targets, were simulated. The simulation runs in a matter of minutes on a single CPU core and produces the trajectories shown in Fig. 4. Thanks to the use of a floor field to attract each group to their specific target, the agents make sensible route choices to their destination, by going around walls and obstacles whenever needed, without being constrained to strictly adhere to a prede-

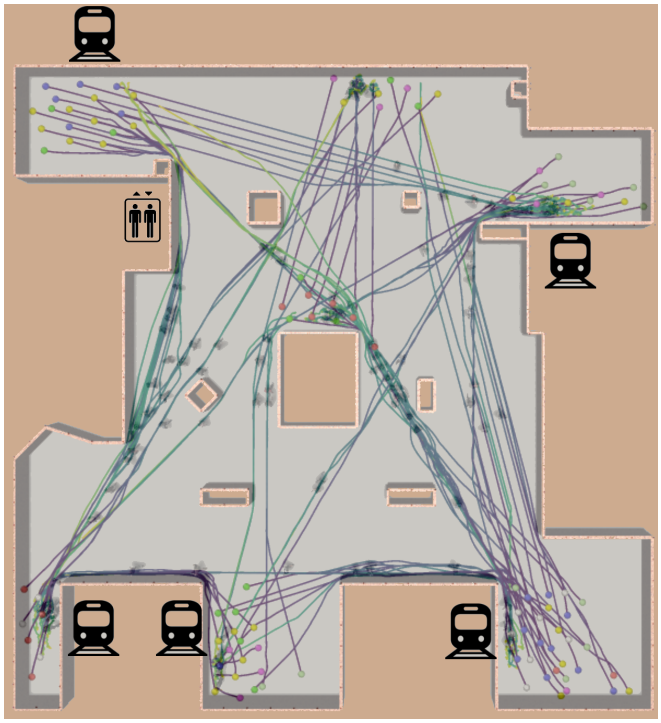

FIG. 4. Navigation of ~ 100 agents, split into 7 groups with distinct target zones, in a complex geometric layout inspired by the ground floor of the Montparnasse train station in Paris, France. The initial positions are marked with colored disks and the solid lines that represent the trajectories evolve from blue to yellow with time.

fined path. Furthermore, the simulated dynamics (shown in the supplemental movie complex_geometry) are qualitatively convincing at the local level, as far as one can judge with the naked eye: the agents succeed in navigating towards their targets in a realistic way, generally avoid collisions with their counterparts and the walls. Still, even closer inspection of the video reveals some hesitancy in the central region when an agent endeavors to cross a group of static pedestrians who have reached their target; this particular situation will be discussed in Sec. III G.

D. Unidirectional flow

Let us now turn to the model's predictions of collective flow properties at higher densities. Specifically, we will investigate the effect of density in unidirectional flow by means of the *speed-density* relation, a broadly used quantitative benchmark for models of pedestrian dynamics. A corridor of length $L_X = 16\,\mathrm{m}$ and width $L_Y = 3\,\mathrm{m}$ is considered, with periodic boundary conditions (PBC) in the horizontal direction. The number of pedestrians inside the corridor is varied from 12 to 144, thus achieving densities ranging from 0.25 and 3 ped/m^2. Each simulation takes 100 seconds to run, the last 75 s of which are used to compute the speed-density relation by averaging the speeds of all agents.

The numerical outcome in Fig. 5 follows the same trends as the empirical data, with a monotonic decay of speed with density that gets sharper around 1.5-2 ped/m^2. It even quantitatively matches with some empirical data, but the dispersion in the latter precludes any bolder statement. The situation at high density $\rho > 2.5\,\mathrm{ped}/m^2$ deserves additional comments. First, the speed is still nonvanishing in this regime, consistently with empirical observations even at (much) higher densities, (far) above 6 ped/m^2 in the pilgrim processions during the Hajj [37] as well as in controlled experiments [40]. Secondly, in the model, the speed seems to level off, possibly excessively. However, it should be noted that pedestrian shapes start to become overly important in this regime. Clearly, the approximation of pedestrians as disks used in this paper for simplicity (to avoid the rotational degree of freedom associated with non-axisymmetric shapes) then reaches its limits. Accordingly, we expect the model predictions to be altered in this regime, should more realistic shapes be simulated.

The spatio-temporal diagrams of speed shown in the lower panels of Fig. 5 for different densities shed light on finer details about the flow dynamics, notably the occurrence of stop-and-go waves in the higher-density regime. This type of instability, wherein a slow or 'jammed', dense phase emerges locally in the unidirectional crowd and propagates upstream, is routinely observed in various forms of traffic and in single-file pedestrian motion [41] when the average spacing between agents is reduced. In corridor flows, spontaneous stop-and-go waves are probably not as systematic, but they have nonetheless be witnessed. For instance, in the controlled experiments of Jin et al. [42] in a ring-like corridor, these waves were observed only for narrow corridors (no wider than 1 meter), allegedly because transverse motion in wider corridors alleviates jamming. Nonetheless, empirical observations before the crowd disaster during the Hajj in 2006 also evidenced stop-and-go waves before turbulence set in, although the packed crowd extended transversely over more than 20 m [37].

In our simulations, no stop-and-go wave was observed at the lowest considered density (label (1), $\rho = 1\,\mathrm{ped}/\mathrm{m}^2$); instead, clusters of fast-walking agents create dark blue streaks, that move downstream at their (high) walking speed. When the density in the corridor increases (label (2), $\rho = 2\,\mathrm{ped}/\mathrm{m}^2$), the spatio- temporal diagrams are qualitatively altered, with regions of halted pedestrians propagating upstream, corresponding to a stop-and-go motion. Interestingly, these backward-travelling waves are conspicuous in our coarse-grained diagrams of speed, but are not apparent when we plot the coarse-grained diagrams of density. Thus, the density indicator used to experimentally detect stop-and-go motion in [42] appears to be less telling than the (longitudinal) speed. At least two factors contribute to explaining

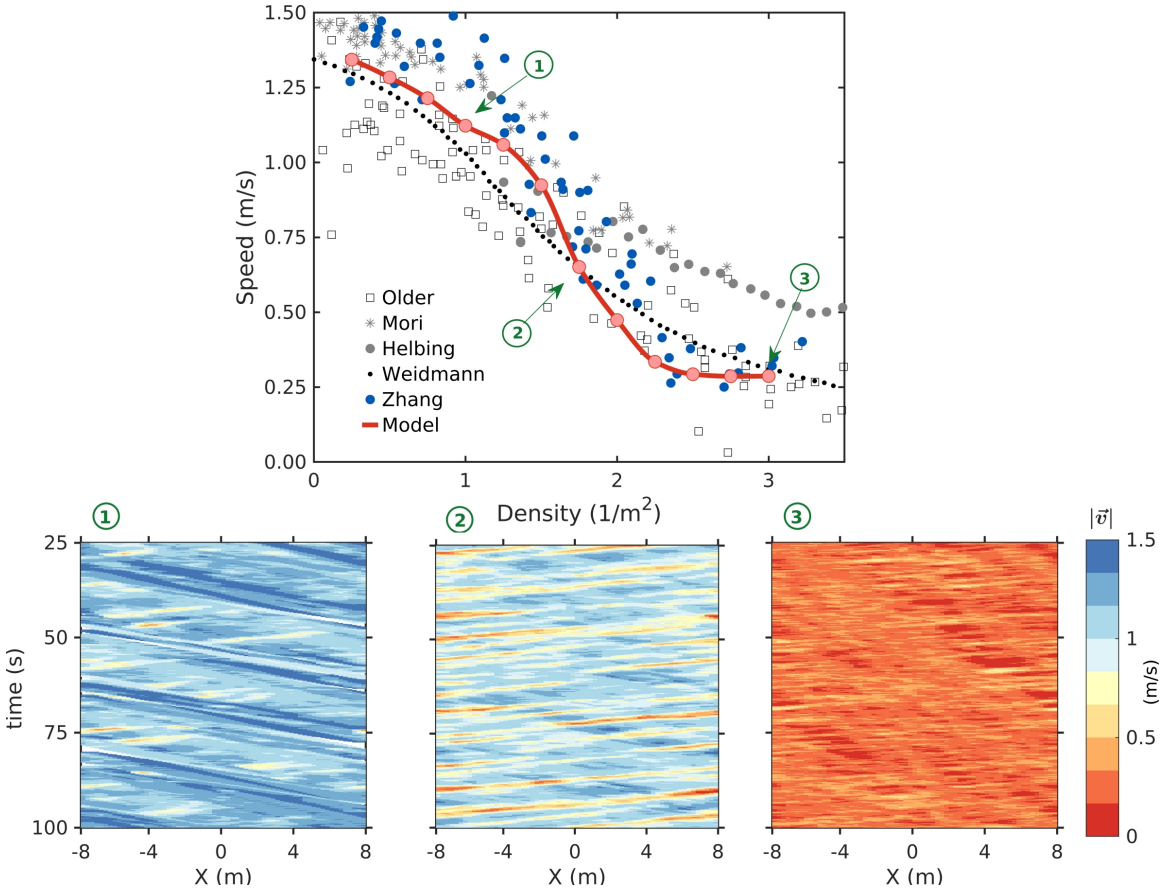

FIG. 5. Unidirectional flow along a corridor of (periodic) length $L_X = 16\,\mathrm{m}$ and width $L_Y = 3\,\mathrm{m}$. (Top) Variation of the simulated mean pedestrian speed with the density, shown along with various experimental data sets (Older [35], Mori and Tsukaguchi [36], Helbing et al. [37], Weidmann [38] and Zhang et al. [39]). (Bottom) Spatio-temporal diagrams of the coarse-grained local speed, represented at different densities, as labeled in the top panel.

the poor sensitivity of the density indicator. First, density is averaged across the corridor width, whereas the jammed phases do not necessarily span the whole corridor width, as we confirmed by direct visualization of the simulated flows (see supplementary movie UniDirFlow); this issue becomes all the more problematic as the corridor is wide. It also comforts the idea [42] that pedestrians in a wide corridor can sometimes evade jammed regions through transverse motion. Secondly, the difference between the density ρ_j in jammed phases and the density ρ_f in flowing ones is fairly small, since the TTC term gets people to brake ahead of a halted person. Because in a strictly one-dimensional setting the conservation of the number of agents imposes that $\rho_f\,(v_f + |w|) \simeq \rho_j\,|w|$ in the steady state, where v_f is the pedestrian speed in the flowing phase and w is the stop-and-go wave speed, the small difference between ρ_f and ρ_j entails a fairly large wave speed $|w| \simeq \frac{\rho_f\,v_f}{\rho_j - \rho_f}$. And, indeed, in Fig. 5(2), we measure a wave speed $|w|$ larger than the free walking speed; we should note that this value exceeds what is typically found for stop-and-go waves in single pedestrian files, where $|w|$ generally lies below $1\,\mathrm{m/s}$ [41]. At even higher densities (label (3), $\rho = 3\,\mathrm{ped/m^2}$), promiscuity slows the flow even more and the dynamics become globally more hampered, but also less bursty.

E. Bidirectional flow

Bidirectional flow exhibits particular features, as compared to the unidirectional case, but is also ubiquitous in daily life, e.g., when two groups of people are found moving in opposite directions in underground corridors, at shopping streets, in commercial streets, etc. Regardless of the type of facility, the system will most probably evolve into a segregated state where people end up forming lanes [43, 44]; such organization reduces collision risks with counter-walking agents and allows people to walk faster. While lane formation has historically been a major benchmark test for any new model, it is noteworthy that this phenomenon is not specific to pedestrian crowds, but is widely found in other active assemblies, and even in simply driven particle systems, such as colloids [45]. Indeed, it is underlain by a generic mechanism: in the non-organized flow, agents undergo small transverse moves after each collision; upon aligning be-

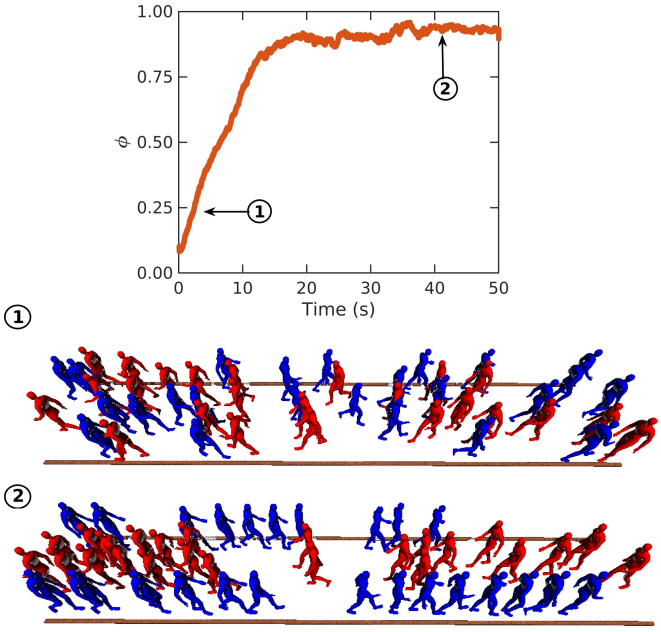

FIG. 6. Lane-formation phenomena in bidirectional flows in a corridor. (Top) Time evolution of the order parameter ϕ (defined in Eq. 16). (Bottom) Snapshots of the crowd at different times, rendered with the CHAOS software developed by INRIA: (1) well-mixed crowd at the beginning of the simulation, (2) crowd structured in counter-walking lanes. The numbers (1) and (2) correspond to the arrows in the top panel. Refer to the main text for the dimensions of the corridor.

hind someone walking in the same direction, these collisions become much less frequent and the aligned state is thus stabilized. Still, the lane-forming state cannot be reached within some pedestrian models in crowded corridors, which leads to deadlocks [46].

To quantify lane formation in our model, we fill the corridor defined in the previous section with N agents, split into an equal number of left and right-moving agents. Following previous works [45, 47], we measure an order parameter

$$\phi = \frac{1}{N}\sum_{i=1}^{N}\phi_i \in [0,1] \text{ with } \phi_i = \left(\frac{N_i^{Same} - N_i^{Diff}}{N_i^{Same} + N_i^{Diff}}\right)^2. \tag{16}$$

where N_i^{Same} and N_i^{Diff} are the number of pedestrians walking on the same line as pedestrian i, respectively in the same direction and in the opposite one, viz.,

$$\begin{aligned} N_i^{Same} &= \{j, |y_j - y_i| < 3\sigma_i/2 \text{ and } \hat{v}_i \cdot \hat{v}_j > 0\} \\ N_i^{Diff} &= \{j, |y_j - y_i| < 3\sigma_i/2 \text{ and } \hat{v}_i \cdot \hat{v}_j < 0\} \end{aligned} \tag{17}$$

where we used $3\sigma_i/2$ as our characteristic length scale (remember that σ_i is the particle radius) previously used and tested in other works [46]. Thus, ϕ measures how stratified the system is, being 0 for a fully mixed state and 1 when lane formation has occurred.

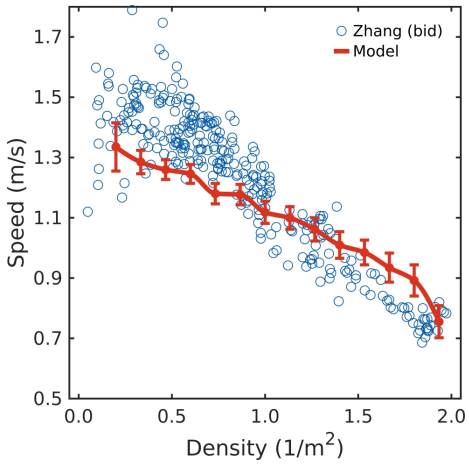

FIG. 7. Variation of the average pedestrian speed with the mean density in a bidirectional corridor flow.

In Fig. 6 we show the temporal evolution of ϕ, effectively finding a transition of the system from a mixed state in the early stages of the simulation (values of ϕ close to 0) to a lane structure where pedestrians are practically segregated with $\phi \sim 1$.

Besides, in the example shown in Fig. 6 ($\rho = 1\,\text{ped/m}^2$), lanes take 10 to 15 seconds to form. Compared to the experimental findings of [40], the simulated lane formation time is somewhat longer than the experimental one for $\rho = 1\,\text{ped/m}^2$, but shorter than for $\rho = 2\,\text{ped/m}^2$; the quantitative comparison should however be taken with a pinch of salt, because the experimental setup was a ring and the initial pedestrian positions also differed.

Finally, the *speed-density* relation for the bidirectional flow is comparable with the unidirectional flow one and is also consistent with experimental measurements, as shown in Fig. 7.

F. Bottleneck flow, evacuation

Let us now break the translational invariance of the corridor by introducing a narrowing (a bottleneck). Streamlines then converge at the narrowing, which generates clogging effects if the flow is dense and the bottleneck is not much wider than a few 'particles'. These effects exist when the particles are grains or animals [48], but are vested with special interest for pedestrians, for they may be critical during egresses or evacuations under emergency conditions. The topic has thus received much attention and some paradoxical effects have been brought to light: While more haste often makes the evacuation quicker, in very competitive settings, higher individual preferential speeds may be counterproductive, leading to long-lived clogs observed empirically as well as experimentally. This is the well-known 'faster-is-slower' effect (FIS), first predicted numerically [49] and then demon-

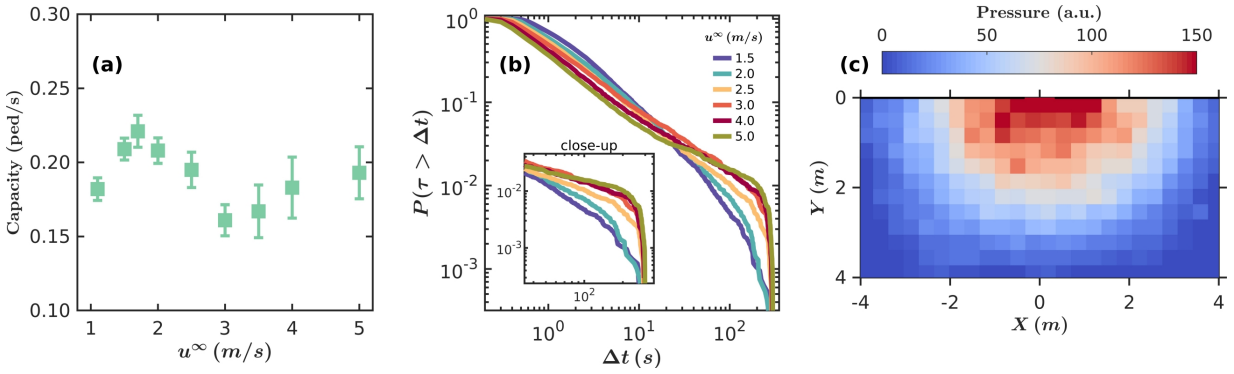

FIG. 8. Evacuation dynamics through a narrow doorway of width $w = 60\,\mathrm{cm}$, centered at $(0, 0)$.**(a)** Dependence of the exit capacity on the preferential speed u^∞; **(b)** Survival function $P(\tau > \Delta t)$ of time gaps between successive egresses; **(c)** Average pressure field due to physical contacts between agents in the vicinity of the exit, for $u^\infty = 3\,\mathrm{m/s}$ and $w = 60\,\mathrm{cm}$.

strated experimentally in a variety of assemblies [48, 50].

Here, we simulate an evacuation from a rectangular room initially filled with 150 randomly positioned agents who strive to egress through a doorway of width w in the middle of one wall. The agents' eagerness to evacuate affects the terminal cost $\mathcal{E}^T$ and, as a consequence, their preferential speed u^∞; the latter will be varied and used as a proxy for eagerness. To avoid deadlocks at the bottleneck, every second the preferential speed of each agent undergoes a small random fluctuation (drawn from a normal distribution of standard deviation 0.2) around its initial, agent-dependent value. Each simulation is replicated around 100 times to collect sufficient statistics to overcome the expected strong fluctuations, and the first and last egresses in each realization are discarded to focus on the quasi-stationary state. Gauging the evacuation efficiency by the exit capacity, i.e., the pedestrian throughput, we show in Fig. 8a that the FIS is retrieved when the door is very narrow, $w = 60\,\mathrm{cm}$: the capacity plummets as soon as u^∞ exceeds $1.7\,\mathrm{m/s}$. In this competitive regime, the total evacuation time T_{evac} exhibits strong fluctuations, rationalized by the (infrequent, but not sporadic) occurrence of very long clogs. These clogs generate large time gaps τ_i between successive egresses, which impact $T_{\mathrm{evac}} = \sum_i \tau_i$. The survival functions $P(\tau > T)$ of the τ_i, represented in a logarithmic plot in Fig. 8b, develop heavy tails, are suggestive of a power-law-like behavior, with flatter and flatter slopes as agents get more and more hurried ($u^{\mathrm{inf}} > 2 - 3\,\mathrm{m \cdot s^{-1}}$), in contrast with the fast decays observed for more placid agents and/or wider doors (Fig. S1f). These features are in perfect agreement with previous experimental findings [50]. Beyond $u^{\mathrm{inf}} \simeq 3\,\mathrm{m/s}$, the flattening trend gets less visible, as the stronger pushing forces counter the clogging phenomenon [51]. In parallel, the *typical* time gaps keep being reduced as the agents move faster; therefore, the capacity starts increasing again with u^∞ (Fig. 8a).

For a slightly larger door, of width $w = 70\,\mathrm{cm}$, the FIS is still noticeable, but not as conspicuous: the non-monotonicity of $J_s(u^\infty$ is only tentatively seen around $u^{\mathrm{inf}} = 4\,\mathrm{m/s}$ (Fig. S1a)). This is broadly in line with the findings of [50], where the FIS was clearly present, but fairly small for a 69cm-wide door (the flow rate in the highly competitive settings was reduced by about 5% smaller compared to the milder settings). For wider doors, $w > 70 - 80\,\mathrm{cm}$, the FIS fades away from our simulations (Fig. S1b,c): Higher preferential speeds u^{inf} lead to higher throughputs.

Aiming for a quantitative comparison, we probe the specific capacities $J_s = \frac{1}{w} \cdot \frac{N}{T_N}$ (where T_N is the duration it took to evacuate N agents in the pseudo-stationary stage of the evacuation), i.e., mean flow rates per unit width of the door. For a 1 m-wide door, our simulations yield $J_s = 1.80\,\mathrm{ped/m/s}$ in normal conditions ($u^{\mathrm{inf}} = 1.5\,\mathrm{m/s}$), right between the estimate $J_s = 1.60\,\mathrm{ped/m/s}$ reported in [52] and the experimental measurements $J_s = 1.85\,\mathrm{ped/m/s}$ and $J_s = 1.90\,\mathrm{ped/m/s}$ in [53] and in [54], respectively. In these last two publications, the specific capacity decreases slightly to around $J_s = 1.8\,\mathrm{ped/m/s}$ and $J_s = 1.6 - 1.7\,\mathrm{ped/m/s}$, respectively, when the door is narrowed to $w = 80\,\mathrm{cm}$; it drops somewhat more significantly in the model, to $J_s = 1.54\,\mathrm{ped/m/s}$, still for $u^{\mathrm{inf}} = 1.5\,\mathrm{m/s}$, but the agreement remains acceptable. For *even* narrower doors it must plainly be conceded that a marked discrepancy arises in the absolute values of the specific capacity, which is around $J_s \approx 1.4\,\mathrm{ped/m/s}$ in the simulations and around $J_s \approx 3.6\,\mathrm{ped/m/s}$ in the experiments. This can easily be explained: Our approximation of pedestrians as frictionless disks is stretched beyond any reasonable limit in a regime dominated by mechanical obstructions and contacts, and in which the shape of agents matters considerably [55]. A better physical description would be attained by refining the mechanical layer using more realistic agent shapes.

Still, the *existence* of a neatly delineated mechanical layer is of great avail as it enables us to define contact forces rigorously, by contrast with models mingling pseudo-forces and real forces. More precisely, the contact force $F_{j \leftarrow i}$ exerted by i on j reads $F_{j \leftarrow i} = -\frac{dU_2}{r_{ij}}$, where U_2 is the Hertzian potential defined previously. If one overlooks variations in the agent's surface area $\mathcal{A}$, the

pressure can then be defined, from a continuum mechanics standpoint, as the sum of contact forces exerted on j times divided by $\mathcal{A}$, viz., $\sum_i F_{ij}/\mathcal{A}$. With this definition, Fig. 8c shows the average pressure field during the evacuation, i.e., the mean pressure felt by agents at each position in space. It is noteworthy that these pressure fields look similar to the density maps measured experimentally in evacuations under similar competitiveness [56].

G. Intruder problem

While competitive evacuations displays many similarities with granular flows through a bottleneck [48], probably owing to the prominence of mechanical contacts, recent experiments have shown that, surprisingly, the granular analogy fares much worse when a group of *static* people is crossed by an 'intruder' [2]: Anticipation and self-propulsion by the pedestrians then play a major role in opening a pedestrian-free tunnel ahead of the intruder via *transverse* displacements, in stark contrast with the granular case. This holds even in the dense regime, where mechanical forces were believed to prevail.

The Social Force Model goes completely amiss in the description of these features [57], which in principle could be captured by our model: agents in the static crowd (whose target position coincides with a circular region of radius the size of the pedestrian and centered on his/her initial position) can anticipate a risk of collision with the intruder and move 'out of harm's way' in advance, by moving away from the expected (linear) intruder's trajectory. In practice, however, we managed to reproduce the density field, with a 'tunnel-like' opening ahead the intruder due to anticipation, but not the purely transverse displacements observed experimentally, even with slight variations of the model or its parameters. In a parallel paper dedicated to this scenario [58], we ascribed the deficiency of most existing agent-based models (including a variant of the present one, see Supplemental Material of [58]) to capture this effect to the fact that in this situation the local navigation is mingled with the tactical planning and that the modeled agents are too short-sighted to achieve this anticipation. For the present model, the alleged origin of this deficiency can be pinpointed more precisely thanks to its transparent derivation: Taking the limit $\delta t \to 0$ in the anticipated cost of motion in Eq. 2 sweeps away the possibility to plan a move that involves a non-constant velocity. A natural way to recover it would be to perform the optimization of the full time-integral in Eq. 2, i.e. with respect to the planned velocity function $\boldsymbol{u}(t')$, $t' \geqslant t$, as in game theory, at the expense of an unbearable computational cost. Mean-field game theory can overcome this intractability, at the expense of losing sight of the discrete nature of pedestrians [58].

Interestingly, this also explains the aforementioned hesitancy of some pedestrians when crossing a group, in the complex scenario studied in Sec. III C.

H. Effect of distracted pedestrians

So far we have shown that key pedestrian dynamics features could be replicated in various settings with a single set of model parameters. Now, we purport to show that the sound physical basis of our model enables us to extend it to an even wider range of situations by straightforwardly adapting its parameters.

To illustrate this, we consider the effect of digital distraction [59–61]. In our increasingly connected societies, with the advent of the Internet of things, more and more pedestrians are indeed looking at their smartphones (or other connected devices) while walking; even near road crossings, more than one pedestrian out of six may be involved in a such an activity (17% in a 2020 study in Athens, Greece [60]). The ensuing distraction impacts their navigation in that it impairs their situational awareness [59, 62], especially when texting or web-browsing [7, 60]. Their walking speed is then reduced [7, 60], as is their eye scanning frequency (by upwards of 25% in controlled outdoor experiments with college students [7]). The whole topic has grown into one of very serious practical relevance insofar as 'smartphone-walking' has entailed a sharp rise in pedestrian injuries. Already in 2010, of the thousands of pedestrians killed in traffic accidents in the US, 3.7% were engaged in a mobile phone activity, as compared to 0.6% in 2004 [59]; the numbers have most probably considerably risen since then, further heightening societal concerns, notably in Japan [63].

While empirical observations and controlled experiments provide much-needed insight into the effect of digital distraction, they reach their limits when it comes to exploring a broad range of situations, in particular on streets; this need can be filled by resorting to models. In order to incorporate distraction effects into our model, we notice that distraction through screens, albeit a complex psychological process, mainly entails that agents less frequently refresh (update) their perception of their surroundings and adapt their motion to it. This is corroborated by the observation that, in a collision avoidance, they tend to turn at the last moment, with a delay of around 0.5 or 1 second in their response, compared to the reference case [64]. This latency effect can readily be transcribed into the model by simply increasing the update time interval of distracted agents ($\delta t = 0.8\,\mathrm{s}$) compared to standard agents ($\delta t = 0.1\,\mathrm{s}$); the walking speed of distracted agents (empirically slower than their counterparts [7]) is set to $u^\infty = 1.2\,\mathrm{m/s}$. Of course, distraction may have other secondary effects that would require further adapting the parameters of the perceived cost, but these are overlooked here.

We now test to what extent this numerical account of distraction is faithful to the experimental observations. To that end, we make use of Murakami et al.'s recent experiments on bidirectional flows in the presence of three digitally distracted agents, i.e., three participants who were instructed to use their smartphone while walking [6]. The researchers observed that their presence ham-

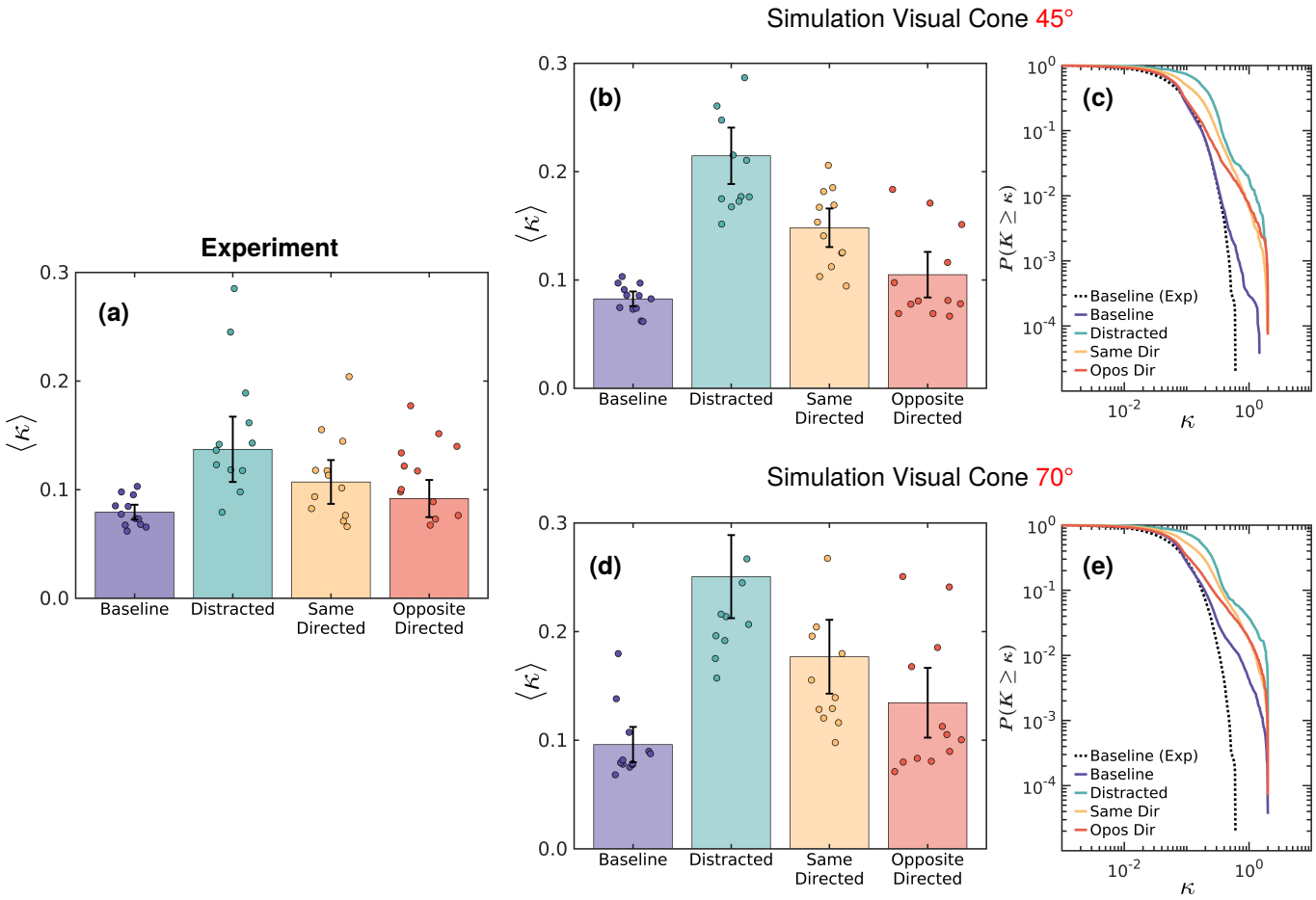

FIG. 9. Impact of distracted pedestrians on the chaoticity of the flow: **(a)** Suddenness of turn κ in the experiments of [6], distinguished between a reference case without distracted agents ('baseline'), the distracted agents, the non-distracted people walking in the same direction and those walking in the opposite direction; **(b)** Suddenness of turn κ computed in our model, for $\theta = 45°$; **(c)** Survival functions $P(K > \kappa)$ in the reference experimental case and for different groups of agents in the simulations. In panels **(d)** and **(e)**, the half-angle of the visual field was restored to its original value, $\theta = 70°$, in the simulations.

pered lane formation and made the flow more chaotic, especially when the three participants were positioned at the front of the group of participants moving in one direction. Quantitatively, they gauged this effect using a suddenness-of-turn observable, which we somewhat amend here to make it invariant under global rotations of the frame:

$$\kappa(t) \hat{=} \left\| \frac{\boldsymbol{e}(t+\delta t) - \boldsymbol{e}(t)}{\delta t} \right\|, \tag{18}$$

where $\boldsymbol{e}(t)$ is the tangential unit vector at time t; κ tends to the geometric curvature in the limit of small δt. In the experimental data (Fig. 9a), larger κ values, hence a more chaotic flow organization insofar as pedestrians prefer walking straight, are found for distracted pedestrians, but also for the participants walking behind them in the same direction (referred to as 'Same Directed' in Fig. 9) and those walking in the opposite direction ('Opposite Directed'), as compared to the reference case with no distracted agents ('Baseline').

Turning to the simulations, we first artificially adorn the simulated trajectories with head sways, because these gait-induced oscillations affect κ. This is done by simply superimposing sine oscillations onto the trajectories $\boldsymbol{z}(t) = x(t) + jy(t)$, viz.

$$\boldsymbol{z}'(t) = \boldsymbol{z}(t) + A\, e^{j\omega t} \boldsymbol{e}_\perp(t). \tag{19}$$

, where the period $\omega = 1.6\,m$ and amplitude $A = 0.04\,m$ were measured in the experimental data of [6]. Once these head sways are taken into account, the average flow chaoticity κ measured experimentally in the reference bidirectional flow (without distracted pedestrians) is recovered in our simulations of an identical setup (Fig. 9d). To go beyond the average value, we computed the full distribution of κ and noticed that a better match between experiments and simulations was reached if the half-angle of the visual field was reduced to $\theta = 45°$ [compare panels (c) and (e) of Fig. 9]; the corresponding mean value is even closer to the experiments. Accordingly, we will set $\theta = 45°$ for all agents, but the trends that we find

are robust if the visual field is not narrowed to such an extent (Fig. 9d).

Introducing smartphone-walking pedestrians in the crowd (especially at the front) substantially increases the chaoticity κ not only for the (few) distracted people, but also for the others, particularly those walking in the same direction. This evolution is surprisingly well captured by our model, wherein digital distraction mostly boils down to having a much longer time δt between updates of the desired velocity (i.e., perception of, and reaction to, the environment): Even though no quantitative coincidence is attained strictly speaking, Fig. 9 shows that the trends and the variations between the pedestrians are depending on their status match the experimental findings. Furthermore, we find that the exacerbated chaoticity is mostly due to the more frequent occurrence of very sudden turns (associated with high κ values), as revealed by the survival functions $P(K > \kappa)$ in Fig. 9c.

IV. CONCLUSION

To summarize, we have put forward a model for pedestrian dynamics that better distinguishes the psychological processes at play from the mechanical ones. In particular, the selection of a desired velocity by each (autonomous) agent is entrusted to a decision-making layer, which optimizes a perceived cost, whereas physical contacts are handled with Newton's equation of motion. Many model parameters can be adjusted based on existing empirical data. Despite the limited number of parameters left for adjustment, the model succeeds in reproducing (often quantitatively) a variety of experimental features over an impressively broad range of situations and densities (without resorting to more specific adjustments, compared to other approaches), overcoming the need for a specific calibration in each regime. These situations include the *speed-density* relations for collision avoidance between several agents, unidirectional and bidirectional flows, bottleneck flows, and navigation in a complex geometry. It can even replicate more exotic phenomena, which data-driven approaches would have struggled to capture, due to the lack of data. Digital distraction through smartphones, which has grown into a major issue for pedestrian safety, is one of them.

Above all, the theoretical delineation highlights the approximations that were made and that would need to be improved for a more faithful description of some scenarios, such as the pedestrian shape, at high densities, and the short-time approximation of the utility function, in situations where the operational dynamics include relatively far-sighted anticipation usually assigned to the tactical level. More broadly speaking, this work opens perspectives for the clarification of the effect of perceptive or decisional faculties on the collective dynamics of self-propelled particles.

ACKNOWLEDGMENTS

The authors are grateful to Chuan-Zhi (aka Thomas) XIE, Hakim BENKIRANE, and Iker ZURIGUEL for their input, to Hisashi MURAKAMI, Claudio FELICIANI, Mohcine CHRAIBI, Daniel PARISI, and Mehdi MOUSSAID for so readily accepting to share their experimental data. This work was partly conducted in the frame of the French-German research project MADRAS funded in France by the Agence Nationale de la Recherche (grant number ANR-20-CE92-0033), and in Germany by the Deutsche Forschungsgemeinschaft (grant number 446168800). I.E. acknowledges Ministerio de Economía y Competitividad (Spanish Government) through Project No. PID2020-114839GB-I00 MINECO/AEI/FEDER, UE and Asociación de Amigos de la Universidad de Navarra for their economical support.

Appendix A: Derivation of the speed energy

The literature in physiology relates the energy expenditure of walking to the rate of oxygen consumption (V_{O_2}), which has a "rest" component and a speed-dependent component:

$$V_{O_2} = V_{O_2}^{(rest)} + V_{O_2}^{(walking)} \tag{S1}$$

We are interested in the second contribution which, in the experimental work of Ludlow et al. [26] is reasonably well fitted by an equation of the form:

$$e^{speed}[u] = K_{s1} + K_{s2}u^2, \text{ for } u \geq u_c \tag{S2}$$

This quadratic relation is consistent with other empirical studies where the energy expenditure of humans in walking motion has been also studied [65]. For the particular case of this work, we discard the base energy consumption (i.e. $e^{speed}[0\,\mathrm{m}\cdot\mathrm{s}^{-1}] = 0$), and subtract this contribution from the experimental data. After this process, we find that the coefficients of the previous equation must be such that:

$$e^{speed}[1.5\,m\cdot s^{-1}] \approx 3\cdot e^{speed}[0.5\,m\cdot s^{-1}] \tag{S3}$$

Finally, we choose to smoothly connect the above e^{speed} expression to 0 so as to avoid discontinuities. This is done with a second-order polynomial:

$$e^{speed}[u] = K_{s3}u + K_{s4}u^2, \text{ for } u < u_c \tag{S4}$$

with coefficients such that they match the higher-speed curve at $u = u_c$, for the single-point value and the derivative. Taking the value of $u_c = 0.1$ and $e^{speed}[1\,m\cdot s] = 1$,

we are able to calculate the value of the 4 parameters associated with both equations, arriving at:

$$\begin{cases} K_{s1} = 0.4 \\ K_{s2} = 0.6 \\ K_{s3} = 7.6 \\ K_{s4} = -35.4 \end{cases} \tag{S5}$$

so that

$$e^{\text{speed}}(u) = \begin{cases} 7.6\,u - 35.4\,u^2 & \text{for } u < 0.1\,\text{m}\cdot\text{s}^{-1} \\ 0.4 + 0.6\,u^2 & \text{for } u \geqslant 0.1\,\text{m}\cdot\text{s}^{-1}. \end{cases} \tag{S6}$$

Appendix B: Derivation of the free walking speed

Isolated agents have no interactions with other agents or the built environment, by definition. It follows that their free walking $\boldsymbol{u}^\infty$ is given by the extremum of $\mathcal{E}(\boldsymbol{u}) = \delta t\Big[e^{\text{speed}}(\boldsymbol{u}) + e^{\text{inertia}}(\boldsymbol{u})\Big] + \mathcal{E}^T(\boldsymbol{r} + \delta t\,\boldsymbol{u})$, viz.,

$$0 = \frac{1}{\delta t}\nabla_{\boldsymbol{u}}\mathcal{E}\Big|_{\boldsymbol{u}=\boldsymbol{u}^\infty} \tag{S1}$$

$$= 2\,\mu\Big(\boldsymbol{u}^\infty - \boldsymbol{v}(t)\Big) + \frac{de^{\text{speed}}}{du}\frac{\boldsymbol{u}^\infty}{u^\infty} + \nabla_{\boldsymbol{r}}\mathcal{E}^T \tag{S2}$$

$$= 2\,\mu\Big(\boldsymbol{u}^\infty - \boldsymbol{v}(t)\Big) + 1.2\,\boldsymbol{u}^\infty - K^T\,\boldsymbol{t} \tag{S3}$$

where we have used the expression of e^{speed} for $u \geqslant 0.1\,\text{m/s}$ from Eq. 4 and defined the unit vector $\boldsymbol{t} = -\nabla_{\boldsymbol{r}}\mathcal{D}/n(\boldsymbol{r})$ pointing towards the target.

Now, an isolated agent quickly reaches their desired velocity $\boldsymbol{u}^\infty$, so that the first term vanishes in steady state. Therefore, we arrive at $\boldsymbol{u}^\infty = \frac{K^T}{1.2}\boldsymbol{t}$, which can be used to set the coefficient K^T from the free-walking speed u^∞.

[1] J. Bruneau and J. Pettré, Energy-efficient mid-term strategies for collision avoidance in crowd simulation, in *Proceedings of the 14th ACM SIGGRAPH/Eurographics symposium on computer animation* (2015) pp. 119–127.

[2] A. Nicolas, M. Kuperman, S. Ibañez, S. Bouzat, and C. Appert-Rolland, Mechanical response of dense pedestrian crowds to the crossing of intruders, Scientific reports **9**, 105 (2019).

[3] M. Aurelius, *Marcus Aurelius: Meditations, Book V* (Oxford University Press, 2013).

[4] A. Gabbana, F. Toschi, P. Ross, A. Haans, and A. Corbetta, Fluctuations in pedestrian dynamics routing choices, arXiv preprint arXiv:2202.02108 (2022).

[5] D. Helbing and P. Mukerji, Crowd disasters as systemic failures: analysis of the love parade disaster, EPJ Data Science **1**, 1 (2012).

[6] H. Murakami, C. Feliciani, Y. Nishiyama, and K. Nishinari, Mutual anticipation can contribute to self-organization in human crowds, Science Advances **7**, eabe7758 (2021).

[7] K. Jiang, F. Ling, Z. Feng, C. Ma, W. Kumfer, C. Shao, and K. Wang, Effects of mobile phone distraction on pedestrians' crossing behavior and visual attention allocation at a signalized intersection: An outdoor experimental study, Accident Analysis & Prevention **115**, 170 (2018).

[8] Y. A. Alaska, A. D. Aldawas, N. A. Aljerian, Z. A. Memish, and S. Suner, The impact of crowd control measures on the occurrence of stampedes during mass gatherings: The hajj experience, Travel medicine and infectious disease **15**, 67 (2017).

[9] J. Van Den Berg, S. Patil, J. Sewall, D. Manocha, and M. Lin, Interactive navigation of multiple agents in crowded environments, in *Proceedings of the 2008 symposium on Interactive 3D graphics and games* (2008) pp. 139–147.

[10] S. Curtis, *Pedestrian velocity obstacles: Pedestrian simulation through reasoning in velocity space*, Ph.D. thesis, The University of North Carolina at Chapel Hill (2013).

[11] D. Bareiss and J. Van den Berg, Generalized reciprocal collision avoidance, The International Journal of Robotics Research **34**, 1501 (2015).

[12] J. Godoy, I. Karamouzas, S. J. Guy, and M. Gini, *C-Nav: Implicit Coordination in Crowded Multi-Agent Navigation*, Tech. Rep. (Tech. Rep, 2016).

[13] M. Shiomi, F. Zanlungo, K. Hayashi, and T. Kanda, Towards a socially acceptable collision avoidance for a mobile robot navigating among pedestrians using a pedestrian model, International Journal of Social Robotics **6**, 443 (2014).

[14] I. Karamouzas, N. Sohre, R. Narain, and S. J. Guy, Implicit crowds: Optimization integrator for robust crowd simulation, ACM Transactions on Graphics (TOG) **36**, 1 (2017).

[15] D. Wolinski, M. C. Lin, and J. Pettré, Warpdriver: context-aware probabilistic motion prediction for crowd simulation, ACM Transactions on Graphics (TOG) **35**, 1 (2016).

[16] D. Helbing and P. Molnar, Social force model for pedestrian dynamics, Physical review E **51**, 4282 (1995).

[17] F. Zanlungo, T. Ikeda, and T. Kanda, Potential for the dynamics of pedestrians in a socially interacting group, Physical Review E **89**, 012811 (2014).

[18] D. Helbing, L. Buzna, A. Johansson, and T. Werner, Self-organized pedestrian crowd dynamics: Experiments, simulations, and design solutions, Transportation science **39**, 1 (2005).

[19] B. Maury and S. Faure, *Crowds in Equations: An Introduction to the Microscopic Modeling of Crowds* (World Scientific, 2018).

[20] Y.-X. Lü, Z.-X. Wu, and J.-Y. Guan, Pedestrian dynamics with mechanisms of anticipation and attraction, Phys-

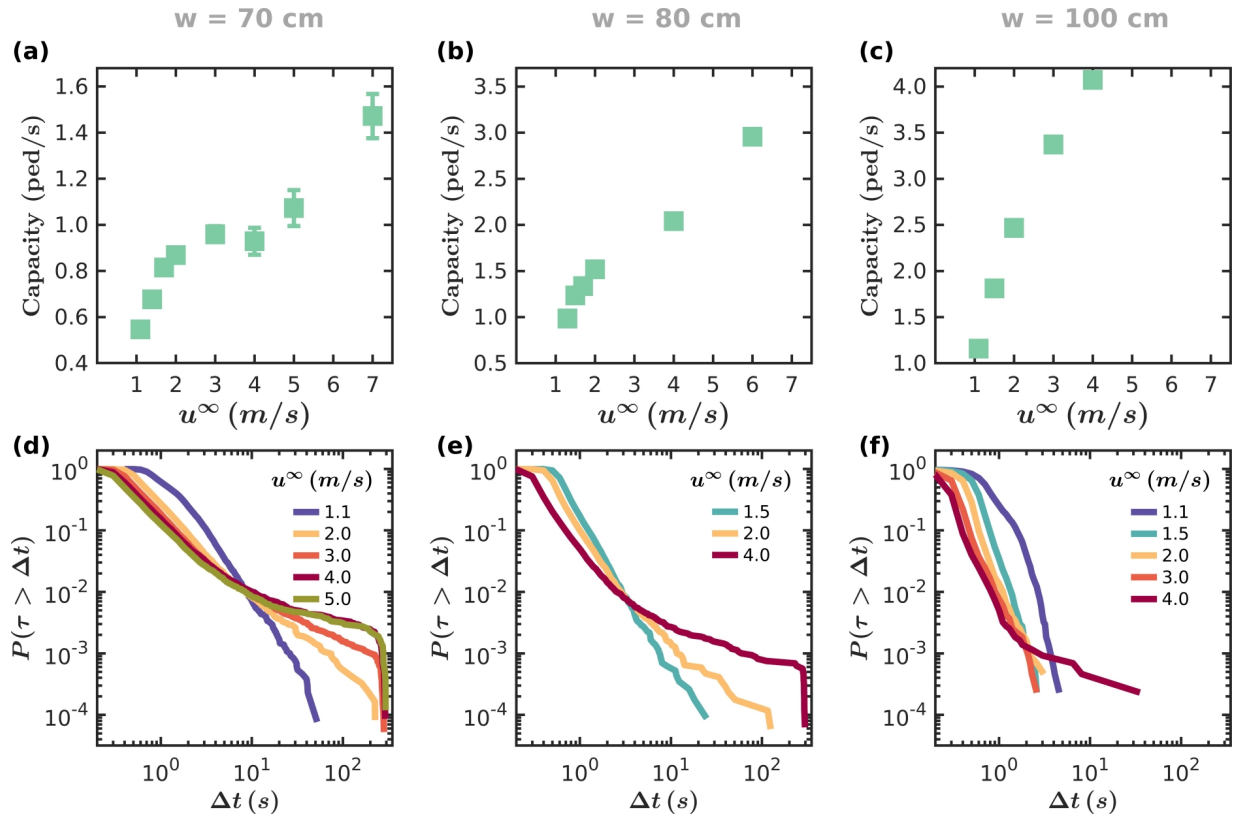

FIG. S1. Evacuation dynamics through bottleneck of different widths, **(a,d)** $w = 70\,\text{cm}$, **(b,e)** $w = 80\,\text{cm}$, **(c,f)** $w = 100\,\text{cm}$. The top row shows the exit capacity as a function of the preferential speed u^∞; the bottom row exposes the survival functions $P(\tau > \Delta t)$ of time gaps between successive egresses.

ical Review Research **2**, 043250 (2020).

[21] I. Karamouzas, B. Skinner, and S. J. Guy, Universal power law governing pedestrian interactions, Physical review letters **113**, 238701 (2014).

[22] M. Moussaïd, D. Helbing, and G. Theraulaz, How simple rules determine pedestrian behavior and crowd disasters, Proceedings of the National Academy of Sciences **108**, 6884 (2011).

[23] A. Nicolas, Dense pedestrian crowds versus granular packings: An analogy of sorts, in *Traffic and Granular Flow 2019* (Springer, 2020) pp. 411–419.

[24] G. Antonini, M. Bierlaire, and M. Weber, Discrete choice models of pedestrian walking behavior, Transportation Research Part B: Methodological **40**, 667 (2006).

[25] A. Corbetta and F. Toschi, Path-integral representation of diluted pedestrian dynamics, in *Complexity Science: An Introduction* (World Scientific, 2019) pp. 329–345.

[26] L. W. Ludlow and P. G. Weyand, Energy expenditure during level human walking: seeking a simple and accurate predictive solution, Journal of Applied Physiology **120**, 481 (2016).

[27] E. T. Hall, *The hidden dimension*, Vol. 609 (Anchor, 1969).

[28] P. Levi, *If this is a man/the truce* (Hachette UK, 2014).

[29] Z. Forootaninia, I. Karamouzas, and R. Narain, Uncertainty models for ttc-based collision-avoidance., in *Robotics: Science and Systems*, Vol. 7 (2017).

[30] D. M. Olsson and L. S. Nelson, The nelder-mead simplex procedure for function minimization, Technometrics **17**, 45 (1975).

[31] Note the subtle technical difference with the acceleration equation used by Moussaid et al. [22]: the desired velocity may change all of a sudden in their approach, whereas abrupt variations of $\boldsymbol{u}^\star$ are penalized in ours.

[32] M. Moussaïd, D. Helbing, S. Garnier, A. Johansson, M. Combe, and G. Theraulaz, Experimental study of the behavioural mechanisms underlying self-organization in human crowds, Proceedings of the Royal Society of London B: Biological Sciences , rspb (2009).

[33] Y. Xiao, Z. Gao, R. Jiang, X. Li, Y. Qu, and Q. Huang, Investigation of pedestrian dynamics in circle antipode experiments: Analysis and model evaluation with macroscopic indexes, Transportation Research Part C: Emerging Technologies **103**, 174 (2019).

[34] Q. Y. Luan, S. B. Liu, Z. J. Fu, and J. Y. Lyu, Experimental and modelling studies of collision avoidance strategy choices and behavioural characteristics in interweaving pedestrian flow, Royal Society open science **9**, 220187 (2022).

[35] S. Older, Movement of pedestrians on footways in shopping streets., Traffic engineering and control **10**, 160 (1968).

[36] M. Mōri and H. Tsukaguchi, A new method for evaluation of level of service in pedestrian facilities, Transportation Research Part A: General **21**, 223 (1987).

[37] D. Helbing, A. Johansson, and H. Z. Al-Abideen, Dy-

namics of crowd disasters: An empirical study, Physical review E **75**, 046109 (2007).
[38] U. Weidmann, *Transporttechnik der Fussgänger. Transporttechnische Eigenschaften des Fussgängerverkehrs, Literaturauswertung*, Tech. Rep. (ETH Zürich, 1992-01).
[39] J. Zhang, W. Klingsch, A. Schadschneider, and A. Seyfried, Transitions in pedestrian fundamental diagrams of straight corridors and t-junctions, Journal of Statistical Mechanics: Theory and Experiment **2011**, P06004 (2011).
[40] C.-J. Jin, R. Jiang, S. Wong, S. Xie, D. Li, N. Guo, and W. Wang, Observational characteristics of pedestrian flows under high-density conditions based on controlled experiments, Transportation research part C: emerging technologies **109**, 137 (2019).
[41] A. Portz and A. Seyfried, Analyzing stop-and-go waves by experiment and modeling, in *Pedestrian and Evacuation Dynamics* (Springer, 2011) pp. 577–586.
[42] C.-J. Jin, R. Jiang, T. Liu, D. Li, H. Wang, and X. Liu, Pedestrian dynamics with different corridor widths: Investigation on a series of uni-directional and bi-directional experiments, Physica A: Statistical Mechanics and its Applications **581**, 126229 (2021).
[43] F. P. Navin and R. J. Wheeler, Pedestrian flow characteristics, Traffic Engineering, Inst Traffic Engr **39** (1969).
[44] K. Yamori, Going with the flow: Micro–macro dynamics in the macrobehavioral patterns of pedestrian crowds., Psychological review **105**, 530 (1998).
[45] J. Dzubiella, G. Hoffmann, and H. Löwen, Lane formation in colloidal mixtures driven by an external field, Physical Review E **65**, 021402 (2002).
[46] Q. Xu, M. Chraibi, and A. Seyfried, Anticipation in a velocity-based model for pedestrian dynamics, Transportation research part C: emerging technologies **133**, 103464 (2021).
[47] J. Chakrabarti, J. Dzubiella, and H. Löwen, Reentrance effect in the lane formation of driven colloids, Physical Review E **70**, 012401 (2004).
[48] I. Zuriguel, D. R. Parisi, R. C. Hidalgo, C. Lozano, A. Janda, P. A. Gago, J. P. Peralta, L. M. Ferrer, L. A. Pugnaloni, E. Clément, *et al.*, Clogging transition of many-particle systems flowing through bottlenecks, Scientific reports **4** (2014).
[49] D. Helbing, I. Farkas, and T. Vicsek, Simulating dynamical features of escape panic, Nature **407**, 487 (2000).
[50] J. M. Pastor, A. Garcimartín, P. A. Gago, J. P. Peralta, C. Martín-Gómez, L. M. Ferrer, D. Maza, D. R. Parisi, L. A. Pugnaloni, and I. Zuriguel, Experimental proof of faster-is-slower in systems of frictional particles flowing through constrictions, Physical Review E **92**, 062817 (2015).
[51] I. M. Sticco, F. E. Cornes, G. A. Frank, and C. O. Dorso, Beyond the faster-is-slower effect, Physical Review E **96**, 052303 (2017).
[52] V. Predtechenskii and A. I. Milinskiĭ, *Planning for foot traffic flow in buildings* (National Bureau of Standards, US Department of Commerce, and the National Science Foundation, Washington, DC, 1978).
[53] T. Kretz, A. Grünebohm, and M. Schreckenberg, Experimental study of pedestrian flow through a bottleneck, Journal of Statistical Mechanics: Theory and Experiment **2006**, P10014 (2006).
[54] A. Seyfried, O. Passon, B. Steffen, M. Boltes, T. Rupprecht, and W. Klingsch, New insights into pedestrian flow through bottlenecks, Transportation Science **43**, 395 (2009).
[55] I. Echeverría-Huarte, I. Zuriguel, and R. Hidalgo, Pedestrian evacuation simulation in the presence of an obstacle using self-propelled spherocylinders, Physical Review E **102**, 012907 (2020).
[56] I. Zuriguel, I. Echeverria, D. Maza, R. C. Hidalgo, C. Martín-Gómez, and A. Garcimartín, Contact forces and dynamics of pedestrians evacuating a room: The column effect, Safety science **121**, 394 (2020).
[57] M. D. Raj and V. Kumaran, Moving efficiently through a crowd: A nature-inspired traffic rule, Physical Review E **104**, 054609 (2021).
[58] T. Bonnemain, M. Butano, T. Bonnet, I. Echeverría-Huarte, A. Seguin, A. Nicolas, C. Appert-Rolland, and D. Ullmo, Pedestrians in static crowds are not grains, but game players, arXiv preprint arXiv:2201.08592 (2022).
[59] J. L. Nasar and D. Troyer, Pedestrian injuries due to mobile phone use in public places, Accident Analysis & Prevention **57**, 91 (2013).
[60] M. Ropaka, D. Nikolaou, and G. Yannis, Investigation of traffic and safety behavior of pedestrians while texting or web-surfing, Traffic injury prevention **21**, 389 (2020).
[61] G. S. Larue and C. N. Watling, Prevalence and dynamics of distracted pedestrian behaviour at railway level crossings: emerging issues, Accident Analysis & Prevention **165**, 106508 (2022).
[62] J. Nasar, P. Hecht, and R. Wener, Mobile telephones, distracted attention, and pedestrian safety, Accident analysis & prevention **40**, 69 (2008).
[63] Y. Takuma, K. R. Krantz, E. Takeaki, and O. Midori, Japan wrestles with dangers of 'smartphone-walking' (2021).
[64] H. Murakami, T. Takenori, C. Feliciani, and Y. Nishiyama, Spontaneous behavioral coordination between pedestrians emerges through mutual anticipation rather than mutual gaze, bioRxiv (2022).
[65] K. B. Pandolf, B. Givoni, and R. F. Goldman, Predicting energy expenditure with loads while standing or walking very slowly, Journal of Applied Physiology **43**, 577 (1977).